

# **Boosting photocatalytic degradation of ethyl acetate by Z-scheme Au-TiO<sub>2</sub>@NH<sub>2</sub>-UiO-66 heterojunction with ultrafine Au as electron mediator**

**Hongli Liu,<sup>ab</sup> Xiaoyi Chang,<sup>ab</sup> Xiaoxun Liu,<sup>ab</sup> Guiying Li,<sup>ab</sup> Weiping zhang,<sup>ab</sup> and  
Taicheng An<sup>\*ab</sup>**

<sup>a</sup> Guangdong Key Laboratory of Environmental Catalysis and Health Risk Control, Guangdong-Hong Kong-Macao Joint Laboratory for Contaminants Exposure and Health, Institute of Environmental Health and Pollution control, Guangdong University of Technology, Guangzhou 510006, China.

<sup>b</sup> Guangdong Engineering Technology Research Center for Photocatalytic Technology Integration and Equipment, Guangzhou Key Laboratory of Environmental Catalysis and Pollution Control, School of Environmental Science and Engineering, Guangdong University of Technology, Guangzhou 510006, China.

\* Corresponding author: **Prof. Taicheng An**

Tel: 86-20-39322298

E-mail: [antc99@gdut.edu.cn](mailto:antc99@gdut.edu.cn)

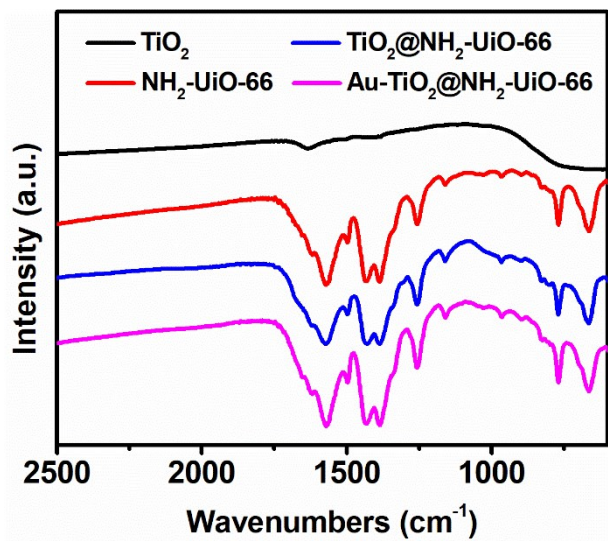


**Fig. S1** FT-IR spectra of  $\text{TiO}_2$ , pure  $\text{NH}_2\text{-UiO-66}$ ,  $\text{TiO}_2@\text{NH}_2\text{-UiO-66}$  and  $\text{Au-TiO}_2@\text{NH}_2\text{-UiO-66}$  in the range of 400-2500  $\text{cm}^{-1}$ .

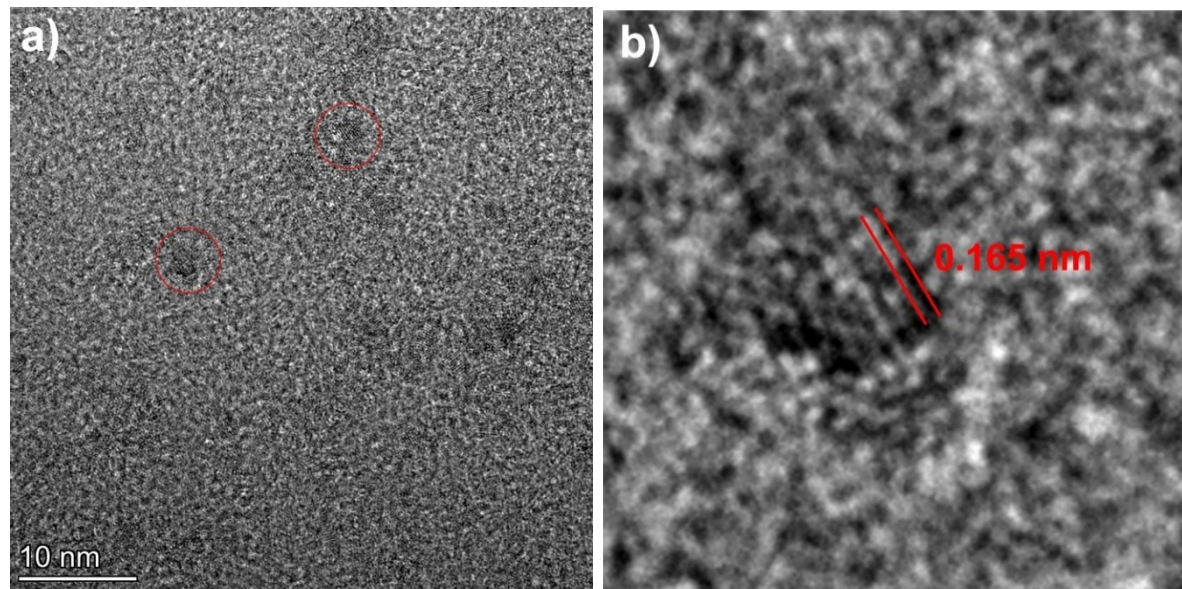


**Fig. S2** TEM images of  $\text{TiO}_2$ .

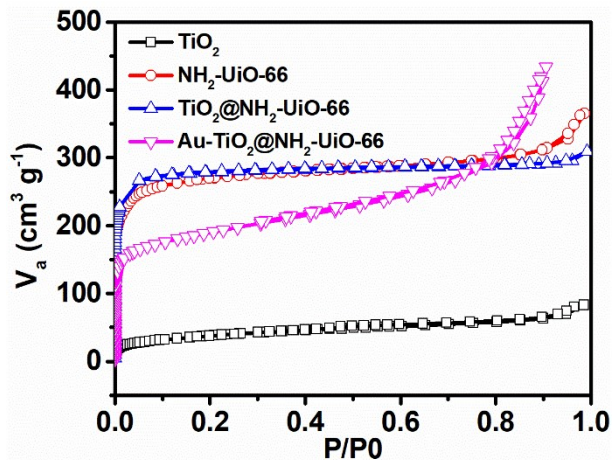


**Fig. S3**  $\text{N}_2$  adsorption-desorption isotherms of  $\text{TiO}_2$ , pure  $\text{NH}_2\text{-UiO-66}$ ,  $\text{TiO}_2@\text{NH}_2\text{-UiO-66}$  and  $\text{Au-TiO}_2@\text{NH}_2\text{-UiO-66}$ .

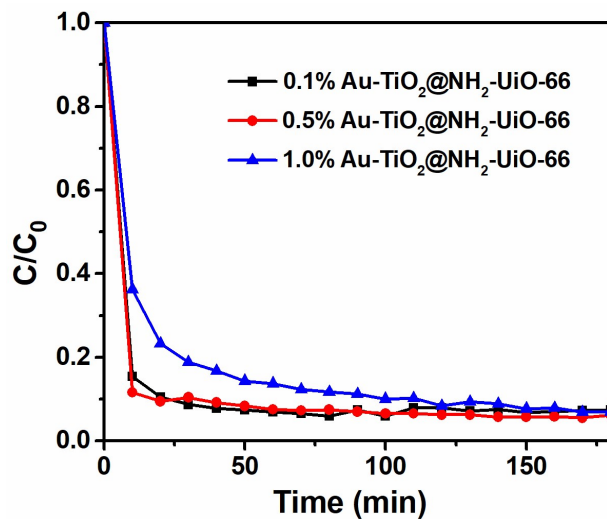


**Fig. S4** Removal efficiencies of ethyl acetate during the photocatalytic oxidation by  $\text{Au-TiO}_2@\text{NH}_2\text{-UiO-66}$  with different Au content.

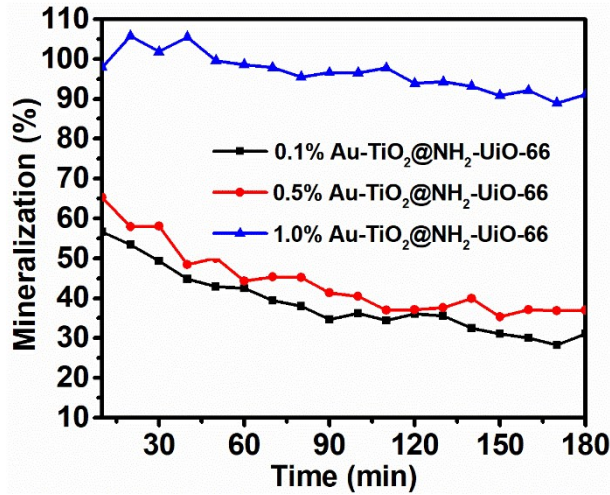


**Fig. S5** Mineralization efficiencies of ethyl acetate during the photocatalytic oxidation by Au-TiO<sub>2</sub>@NH<sub>2</sub>-UiO-66 with different Au content.

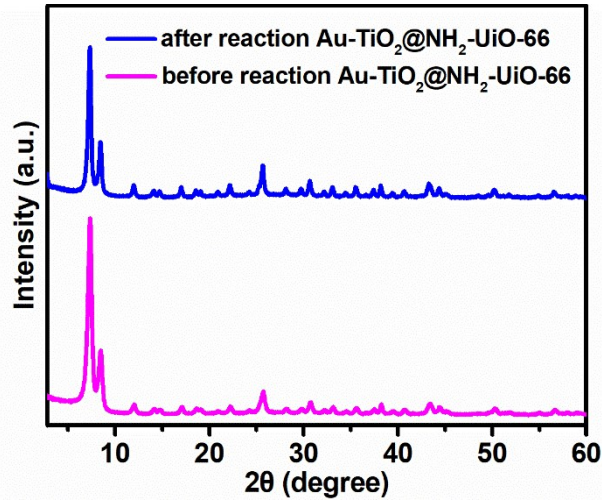


**Fig. S6** Powder XRD patterns of before reaction (a)and after reaction Au-TiO<sub>2</sub>@NH<sub>2</sub>-UiO-66 samples.

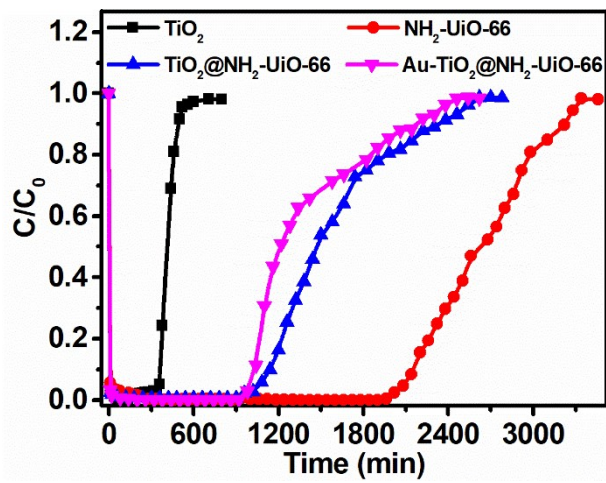


**Fig. S7** Adsorption kinetic curves of ethyl acetate on  $\text{TiO}_2$ , pure  $\text{NH}_2\text{-UiO-66}$ ,  $\text{TiO}_2@\text{NH}_2\text{-UiO-66}$  and  $\text{Au-TiO}_2@\text{NH}_2\text{-UiO-66}$ .

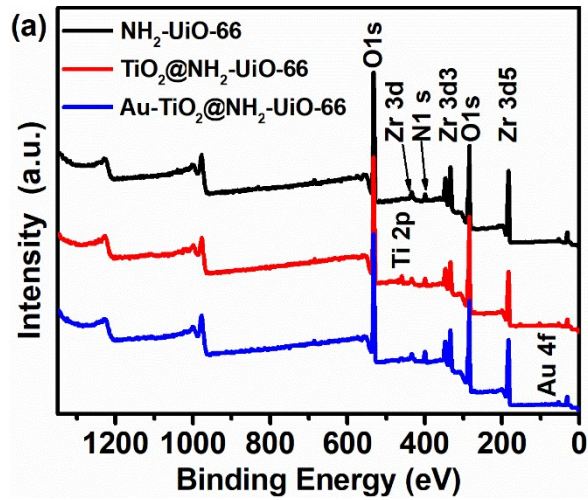


**Fig. S8** XPS survey spectra of pure  $\text{NH}_2\text{-UiO-66}$ ,  $\text{TiO}_2@\text{NH}_2\text{-UiO-66}$  and  $\text{Au-TiO}_2@\text{NH}_2\text{-UiO-66}$  samples, respectively.

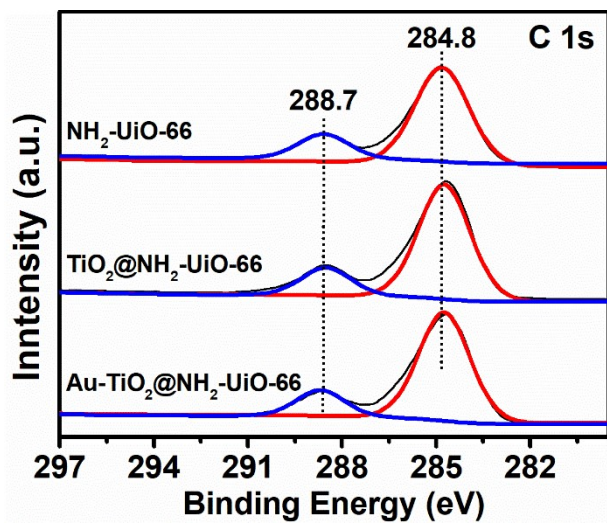


**Fig. S9** XPS spectra of C 1s for pure  $\text{NH}_2\text{-UiO-66}$ ,  $\text{TiO}_2@\text{NH}_2\text{-UiO-66}$  and  $\text{Au-TiO}_2@\text{NH}_2\text{-UiO-66}$  samples, respectively

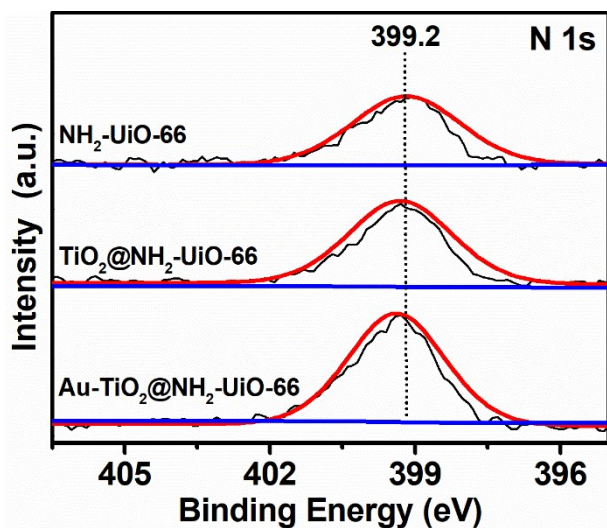


**Fig. S10** XPS spectra of N 1s for pure  $\text{NH}_2\text{-UiO-66}$ ,  $\text{TiO}_2@\text{NH}_2\text{-UiO-66}$  and  $\text{Au-TiO}_2@\text{NH}_2\text{-UiO-66}$  samples, respectively

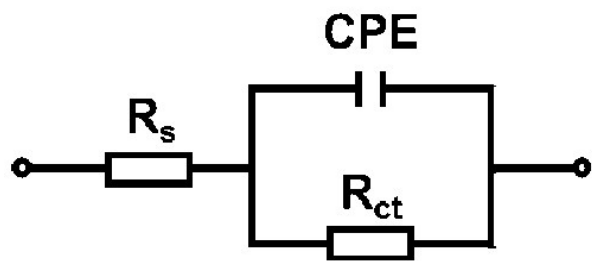


**Fig. S11** the equivalent electrical circuit for EIS.

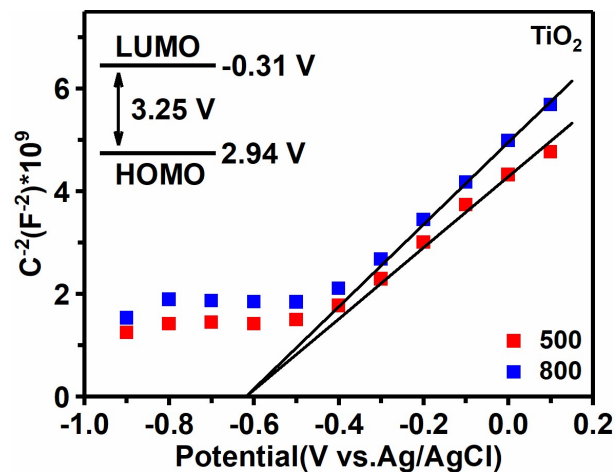


**Fig. S12** Mott-Schottky plots for  $\text{TiO}_2$  at frequencies of 500 and 800 Hz.

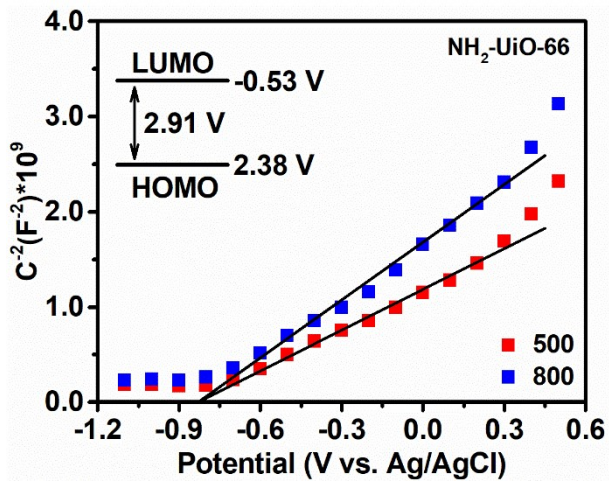


**Fig. S13** Mott-Schottky plots for pure  $\text{NH}_2\text{-UiO-66}$  at frequencies of 500 and 800 Hz.

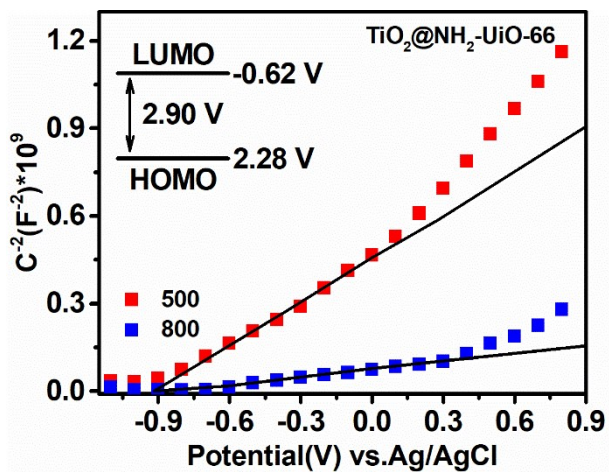


**Fig. S14** Mott-Schottky plots for  $\text{TiO}_2@\text{NH}_2\text{-UiO-66}$  at frequencies of 500 and 800 Hz.

**Table S1** Characterization results of the samples by N<sub>2</sub> adsorption-desorption.

Sample	S <sub>BET</sub> (m <sup>2</sup> g <sup>-1</sup> )	S <sub>Langmuir</sub> (m <sup>2</sup> g <sup>-1</sup> )	V <sub>pore</sub> (cm <sup>3</sup> g <sup>-1</sup> )
TiO <sub>2</sub>	126.9	134.0	0.07
NH <sub>2</sub> -UiO-66	910.3	1275.6	0.41
TiO <sub>2</sub> @NH <sub>2</sub> -UiO-66	725.4	807.1	0.36
Au-TiO <sub>2</sub> @NH <sub>2</sub> -UiO-66	609.1	627.4	0.33

**Table S2** Fitted TRPL parameters of TiO<sub>2</sub>, TiO<sub>2</sub>@NH<sub>2</sub>-UiO-66 and Au-TiO<sub>2</sub>@NH<sub>2</sub>-UiO-66.

Sample	$\tau$ (ps)	$\tau_1$ (ns)	A <sub>1</sub> (%)	$\tau_2$ (ns)	A <sub>2</sub> (%)	$\tau_3$ (ps)	A <sub>3</sub> (%)
NH <sub>2</sub> -UiO-66	358.00	3.06	14.04	22.39	10.90	273.89	75.06
TiO <sub>2</sub> @NH <sub>2</sub> -UiO-66	100.47	2.92	13.01	23.71	12.17	75.55	74.82
Au-TiO <sub>2</sub> @NH <sub>2</sub> -UiO-66	88.75	2.92	14.03	24.01	11.24	70.59	74.73

**Table S3** Fitting results for equivalent electrical circuits of different samples

Sample	Rs ( $\Omega$ )	Rct ( $k\Omega$ )	CPE ( $\mu F$ )
TiO <sub>2</sub>	43.93	11.47	10.42
Pure MOF	44.32	15.21	9.73
TiO <sub>2</sub> @MOF	50.12	3.67	10.94
Au-TiO <sub>2</sub> @MOF	46.99	2.89	12.19

**Table S4** Activity comparison between Au-TiO<sub>2</sub>@NH<sub>2</sub>-UiO-66 and the other typical MOF based photocatalysts for the photocatalytic degradation of VOCs

Catalyst	Dose (g)	VOCs Concentration	Flow rate (mL/min)	Light source	Con. (%)	Mineralization rate (%)	Time (min)	Stability	Ref.
GC-N-TiO <sub>2</sub> 46 wt%	0.1	toluene, 25 ppmv	100	300W, Xe lamp	70	76	1440	Stable, 24 h	1
TiO <sub>2</sub> @NH <sub>2</sub> -MIL-125	0.1	methanal, 10 ppmv	600	125W, Mercury lamp	90	>99	2880	Stable, 122 h	2
Mesoporous TiO <sub>2</sub>	1.0	benzene, 25 ppmv	1000	4W, 254 nm, UV lamp	90	15	130	90.0 % to 60.4% (18 h)	3
Pd-TiO <sub>2</sub>	-	toluene, 105 ppmv	800	10 W, Mercury lamp	58	23	2280	Stable, 40 h	4
MIL-100(Fe)/ $\alpha$ -Fe <sub>2</sub> O <sub>3</sub> -15 5 wt%	0.095	o-xylene, 50 ppmv	10	250 W, Xe lamp	100	-	300	Stable, 20 h	5
TiO <sub>2</sub> @NH <sub>2</sub> -UiO-66	0.1	styrene, 30 ppmv	35	300W, Xe lamp	99	35	600	Stable, 10 h	6
Ni-MOF/NF	2×3 cm	ethyl acetate, 70 ppmv	35	300W, Xe lamp	90	41	360	Stable, 6 h	7
1 wt% Au-TiO <sub>2</sub> @NH <sub>2</sub> -UiO-66	0.1	n-butanol, ethyl acetate	70	300W, Xe lamp	94.6	85	360	Stable, 6 h	This work

## References

1. J. Qin, J. Wang, J. Yang, Y. Hu, M. Fu and D. Ye, Metal organic framework derivative-TiO<sub>2</sub> composite as efficient and durable photocatalyst for the degradation of toluene, *Appl. Catal. B: Environ.*, 2020, **267**, 118667.
2. Q. Huang, Y. Hu, Y. Pei, J. Zhang and M. Fu, In situ synthesis of TiO<sub>2</sub>@NH<sub>2</sub>-MIL-125 composites for use in combined adsorption and photocatalytic degradation of formaldehyde, *Appl. Catal. B: Environ.*, 2019, **259**, 118106.
3. J. Ji, Y. Xu, H. Huang, M. He, S. Liu, G. Liu, R. Xie, Q. Feng, Y. Shu, Y. Zhan, R. Fang, X. Ye and D. Y. C. Leung, Mesoporous TiO<sub>2</sub> under VUV irradiation: Enhanced photocatalytic oxidation for VOCs degradation at room temperature, *Chem. Eng. J.*, 2017, **327**, 490.
4. J. Kim, P. Zhang, J. Li, J. Wang and P. Fu, Photocatalytic degradation of gaseous toluene and ozone under UV<sub>254+185</sub> nm irradiation using a Pd-deposited TiO<sub>2</sub> film, *Chem. Eng. J.*, 2014, **252**, 337.
5. L. Chen, X. Wang, Z. Rao, Z. Tang, Y. Wang, G. Shi, G. Lu, X. Xie, D. Chen and J. Sun, In-situ synthesis of Z-Scheme MIL-100(Fe)/α-Fe<sub>2</sub>O<sub>3</sub> heterojunction for enhanced adsorption and Visible-light photocatalytic oxidation of O-xylene, *Chem. Eng. J.*, 2021, **416**, 129112.
6. P. Yao, H. Liu, D. Wang, J. Chen, G. Li and T. An, Enhanced visible-light photocatalytic activity to volatile organic compounds degradation and deactivation resistance mechanism of titania confined inside a metal-organic framework, *J. Colloid. Interf. Sci.*, 2018, **522**, 174.
7. X. Ding, H. Liu, J. Chen, M. Wen, G. Li, T. An and H. Zhao, In situ growth of well-aligned Ni-MOF nanosheets on nickel foam for enhanced photocatalytic degradation of typical volatile organic compounds, *Nanoscale*, 2020, **12**, 9462.